Multidetector study of primary projectilelike fragments in the reaction $^{40}Ca + ^{nat}Cu$ at 35 MeV/nucleon

A. Lleres, A. Giorni, H. Elhage, M. E. Brandan,* A. J. Cole, P. Désesquelles, D. Heuer, A. Menchaca-Rocha,* and J. B. Viano
Institut des Sciences Nucléaires, IN2P3-CNRS et Université Joseph Fourier, 53 avenue des Martyrs, F-38026 Grenoble Cedex, France

F. Benrachi, B. Chambon, B. Cheynis, D. Drain, and C. Pastor
Institut de Physique Nucléaire, IN2P3-CNRS et Université Claude Bernard, 43 boulevard du 11 Novembre 1918, F-69622 Villeurbanne Cedex, France

(Received 29 July 1993)

Properties of projectile fragments produced in peripheral and midperipheral collisions in the reaction $^{40}Ca + ^{nat}Cu$ at 35 MeV/nucleon were investigated using the AMPHORA multidetector. A reconstruction of the primary projectilelike fragments enabled simultaneous determination of their excitation energy and angular momentum. These quantities are in good agreement with predictions of simple macroscopic and microscopic collision models. Partition of excitation energy between primary projectile and targetlike fragments is discussed. The multiplicity and charge distributions of the primary projectilelike fragment deexcitation products are fairly well reproduced by a statistical binary-decay model.

PACS number(s): 25.70.Pq, 25.70.Mn

I. INTRODUCTION

Current understanding of projectilelike fragment (PLF) production in peripheral and midperipheral heavy ion collisions at intermediate energies has been obtained mainly from inclusive or semiexclusive measurements, which have been used to test parametrized models of the production mechanism of the excited primary projectilelike fragments (PPLF's) and their subsequent decay [1–6]. At low incident energies (below 15 MeV/nucleon) conversion of entrance channel kinetic energy and angular momentum into thermal and rotational energies of the primary projectile and targetlike fragments are thought to be dominated by a one-body mechanism [7,8]. At higher incident energies the Pauli principle becomes less effective in suppressing nucleon-nucleon collisions and schematic microscopic models based on nucleon-nucleon collisions [9,10] have been quite successful in explaining total reaction cross sections and fragment yields, as well as PLF energy and angular distributions.

Primary projectilelike fragments with excitation energies up to 6–7 MeV/nucleon can be produced in very inelastic reactions at incident energies of the order of 30–35 MeV/nucleon [6,11]. It is interesting to understand how the decay mechanism of such nuclei is influenced by temperature and rotation. At low excitation energies, the emitted light particles and projectile residues are well described by statistical evaporation models [12,13] based on the multistep Hauser-Feshbach formalism [14]. For higher excitation energies, such a formalism becomes inadequate, since the emission of intermediate mass fragments may compete significantly with light-particle emission [11]. Sequential binary statistical decay models [15] based on the transition-state formalism [16] are used to describe the deexcitation of such highly excited nuclei. At very high excitation energies, the time scale for particle emission may become comparable with typical equilibration times [17], and simultaneous multifragmentation mechanisms have been proposed [18,19].

The use of a multidetector in the experimental investigation provides a qualitative advance in the sense that, for completely exclusive measurements, it is possible (in favorable kinematic configurations) to separate projectilelike and targetlike fragments and to reconstruct the primary projectilelike fragments, thus gaining direct access to their kinetic characteristics. Furthermore, properties of the observed particles in the PPLF center-of-mass reference frame yield information on the initial internal PPLF thermal and rotational energies and on the temperatures characteristic of the emitted light particles.

This work is a continuation of a study of the reaction $^{40}Ca + ^{nat}Cu$ at 35 MeV/nucleon with the AMPHORA array, which was first mainly devoted to analysis of charge partitions associated with the decay of excited calcium nuclei [11]. By comparing the measured charge partitions with a simple percolation model, it was shown that the physical events at excitation energies close to 5 MeV/nucleon have similar characteristics to those obtained from the percolation simulation with a bond-breaking probability equal to the critical value. However, from analysis of momentum ellipsoids, no evidence for a change in disintegration mechanism with increasing excitation energy, which could be associated with the passage through the critical region, was found.

*Permanent address: IFUNAM, A.P. 20-364, Mexico 01000 DF, Mexico.

The experimental setup is presented in the following section. In Sec. III, selection of peripheral (binary) collisions is described, and the technique for the event by event reconstruction of the PPLF is presented. This makes use of a simulation of the detector response (which needs, of course, a simulation of the nucleus-nucleus collisions). Such simulations are important for the verification of the event selection criteria and of the reconstruction technique. In Sec. IV we present an analysis of the PPLF properties, which includes excitation energy and angular momentum, extracted from the particle center-of-mass energies and angular distributions. In Sec. V we make some comparison of our data with simple macroscopic and microscopic collision model predictions and with statistical binary-decay calculations. Finally in the last section we summarize and discuss our findings.

II. EXPERIMENTAL SETUP

The experiment was carried out using the AMPHORA multidetector [20] installed at the SARA heavy ion accelerator in Grenoble. The beam was ^{40}Ca at 35 MeV/nucleon. The target was a self-supporting natural copper foil of 500 μg/cm^2 thickness. AMPHORA is a multidetector, which covers 82% of 4π sr and is made up of 140 CsI scintillator cells which provide mass and charge identification for light particles ($Z \leq 2$). Thin plastic scintillator foils (100 and 200 μm thickness) were set on the forward detectors (angles ranging from 4° to 57°). They provided charge identification up to $Z=20$ with unit resolution for $Z \leq 9$ and better than ± 2 units for $Z > 9$. The identification technique was described in some detail in our earlier paper [11]. Energy calibration for CsI detectors was made using a thorium source, a 24 MeV α-particle beam and punch-through energies. For plastic+CsI detectors the calibration parameters of Stracener *et al.* [21] were used. For the wall detectors (4°–17°) the time of flight was measured using the cyclotron frequency as the start signal (the flight distance was 140 cm). Light particles with very low velocity were thus identified in charge (no mass separation). Higher charges ($Z \geq 3$) could not be identified from the time-of-flight and plastic light measurements. The detection thresholds for plastic+CsI detectors without time of flight were imposed by the thickness of the plastic foils, which was 100 μm for the rings set at 31° and 47° and 200 μm for the more forward rings. For the 200 μm case, the thresholds reach 4 MeV for protons, 14 MeV for α particles and 6–10 MeV/nucleon for heavier ions ($Z=5-15$). For the CsI crystals, the energy thresholds were 4 MeV for protons, 7 MeV for α particles, and 10 MeV for lithium particles.

III. EVENT SELECTION AND PPLF RECONSTRUCTION

Appropriate selection criteria on global variables are needed to select, among the detected events (all impact parameters), those arising from binary (peripheral and semiperipheral) reactions. Such criteria depend strongly on the kinematical and dynamical features of the reaction under study as well as on the characteristics (geometry, granularity, detection thresholds, and identification accuracy) of the detection array [22]. To investigate these problems, two different models have been used to simulate the nucleus-nucleus interaction (peripheral and central collisions) and the subsequent decay of the produced primary excited systems, and a simulator has been developed to describe the AMPHORA response.

After selection of peripheral collisions, the PPLF was reconstructed event by event. The checking of the validity of the adopted reconstruction method was also carried out by simulation of the collisions and of the detector response.

The first employed model is the microscopic Monte Carlo code CASCADITA [23]. In this simulation, the nucleus-nucleus interaction is assumed to be dominated by nucleon-nucleon collisions occurring in the overlapping region of the two colliding nuclei. The influence of the mean field is taken into account via a nucleus-nucleus deflection function derived from an elastic scattering optical model. Every nucleon scattered twice is assumed to be thermalized and captured by the scattering nucleus. This leads to an exchange of mass, energy, and linear momentum between the projectile and target nuclei (angular momentum transfer is not taken into account). The primary projectile and targetlike fragments subsequently decay through a statistical binary process. Particles are emitted isotropically in the center-of-mass reference frame of the emitting source.

Although CASCADITA allows the fusion between the two primary fragments if their relative energy is below the fission barrier, such simulated events are very scarce for the reaction ^{40}Ca+^{nat}Cu at 35 MeV/nucleon. Indeed, experimental evidence for the formation of incomplete fusion nuclei exists for similar systems (fusion reactions represent about 4% of the total cross section) [24]. Thus, another simulation code (CCP), which treats incomplete fusion reactions, has been written. The code CCP includes the preequilibrium emission of neutrons and protons and calculates the deexcitation of the compound system by means of a sequence of statistical binary decays [25]. The preequilibrium nucleons are emitted from a source moving with half the projectile velocity. The average number of preequilibrium nucleons is estimated according to the Blann model [26], and their momenta are assumed to follow a Boltzmann distribution of temperature 7 MeV [27]. For the reaction under study, the Blann model predicts the ejection of 22 preequilibrium nucleons. This value is in agreement with linear momentum transfer systematics for similar systems [24]. The CCP decay step roughly takes into account the in-plane focusing effect of the compound-nucleus angular momentum.

The AMPHORA response function has been computed by the code SIR, which includes a geometrical description of the detectors, the energy thresholds for each particle, and the identification constraints for each detector type. The effect of the geometrical efficiency and energy thresholds of the 4π AMPHORA array on measurements on symmetric and inverse kinematics systems at energies near 35 MeV/nucleon was discussed in a previous work

[22]. The simulated events created by the models are thus filtered by the detector response and an event by event set of data is generated.

The analysis of the simulated-filtered (CASCADITA and CCP) events shows that the inelastic (binary) collisions can be selected by constraints on the total detected charge Z_{tot} and on the total measured parallel linear momentum P_{tot}, which are the following:

$$P_{tot} \geq 6 \text{ GeV}/c \quad \text{and} \quad Z_{tot} \geq 20 \, . \tag{1}$$

The Z_{tot} vs P_{tot} distributions obtained for the CCP and CASCADITA calculations are plotted in Fig. 1. The experimental plot is also presented in Fig. 1. The total charge of the system is 49 (20 for the projectile), and the total linear momentum is 10.2 GeV/c. The condition on P_{tot} allows the rejection of almost all the incomplete fusion events (the CCP calculation shows that less than 1% of the events have a total parallel linear momentum greater than 6 GeV/c). With the condition on Z_{tot}, binary (CASCADITA) events, where most of the products associated with the PPLF are detected, are selected. In these events, a few particles coming from the decay of the primary targetlike fragments (PTLF's) are also detected, as well as some preequilibrium nucleons. The correlation between the total detected charge coming from the PPLF decay and the PPLF charge is plotted in Fig. 2 without 2(a) or with 2(b) the condition on Z_{tot}. With such a condition, we observe that very incomplete PPLF events are rejected and that there is a strong correlation between the total detected charge and the charge of the primary projectilelike fragment. The CASCADITA simulation shows

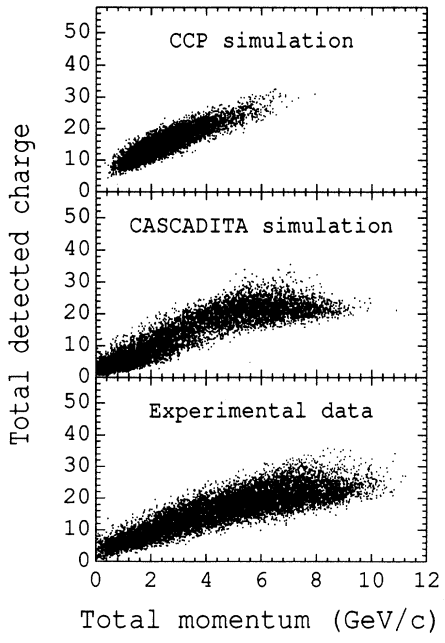

FIG. 1. Plots of total detected charge versus total measured parallel linear momentum from CCP simulation, CASCADITA simulation, and experimental data. The simulated events are filtered by the AMPHORA response function.

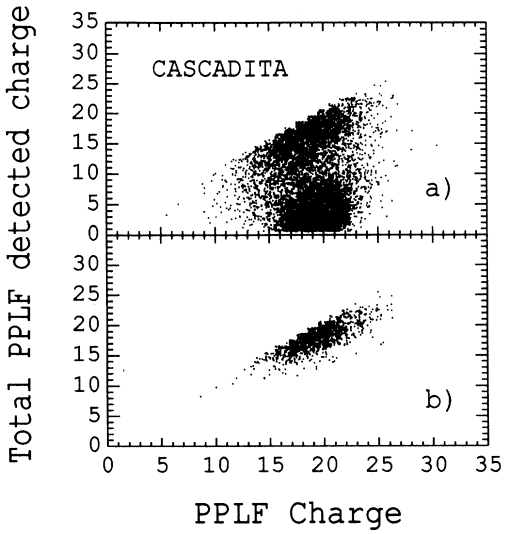

FIG. 2. Correlation between the total detected charge of the PPLF decay products and the PPLF charge, given by the CASCADITA simulation (a) without condition and (b) with the condition on the total detected charge $Z_{tot} \geq 20$. Both spectra correspond to the same sample of events.

that the detection efficiency on the charge of the particles coming from the PPLF is on the average around 90% (the mean charge of the PPLF—before filtering—is 19.5, whereas the total detected charge of the PPLF—after filtering—is, on the average, 17.8); for the PTLF this value is about 15%. The experimental sample selected by criteria (1) represents about 25% of the recorded events. See Refs. [22,28] for a more detailed discussion about the AMPHORA filter effects on experimental and simulated global variables.

As the preceding constraints select events where the observed particles come from both the deexcitation of the PPLF and PTLF (and include also preequilibrium particles), we have developed a method to separate the PPLF particles from those coming from the other emission sources [29]. This method is essentially the same as the one presented in our previous work [11]; it presents some minor changes, which are described below. The CASCADITA simulation shows that the fragment of charge $Z \geq 3$ having the largest linear momentum is generally the PPLF decay residue [with conditions (1), the projectilelike residue is almost always present]. The velocity of such a residue defines the velocity $\mathbf{v}_\Omega$ of the PPLF center of mass. The method of selecting the particles coming from the deexcitation of the PPLF is based on the hypothesis that all these particles belong (in the velocity space) to a sphere centered on the velocity $\mathbf{v}_\Omega$. Analysis of experimental velocity correlation functions between light particles and projectilelike residues leads to the choice of a maximum relative velocity v_{max} (sphere radius) of 5 cm/ns for protons and 4 cm/ns for heavier particles [29]. In addition, we assume that all particles emitted in the forward direction and having a velocity greater than v_{max} are emitted by the PPLF. Thus, if v_{rel} is the relative velocity of the particles with respect to the PPLF

center-of-mass reference frame, the criteria for their adherence to the PPLF are the following:

$$\mathbf{v}_{\mathrm{rel}}\cdot\mathbf{v}_{\Omega}<0$$

and

$$v_{\mathrm{rel}}\leq 5 \text{ cm/ns (protons), 4 cm/ns (others)} \quad (2)$$

or

$$\mathbf{v}_{\mathrm{rel}}\cdot\mathbf{v}_{\Omega}\geq 0 .$$

These selection conditions enable us to completely reconstitute the PPLF. Its center-of-mass velocity $\mathbf{v}_{\Omega}$ is again calculated by taking into account all the particles attributed to the PPLF. The obtained experimental charge distribution of the reconstituted PPLF is plotted in Fig. 3 (its mean value is 18.6). Figure 4 shows the correlation between the PPLF detected charge given by the CASCADITA simulation (after filtering, mean value 17.8) and its reconstructed charge, which is, on the average, 18.9 (after filtering and reconstruction). For reconstructed charges $Z_{\mathrm{PPLF}}\leq 20$, we obtain a contamination of about 10% of the charge, which is due to the PTLF and preequilibrium sources (contamination only by light particles). For charges greater than 20, the contamination becomes more important and increases with the charge (for $Z_{\mathrm{PPLF}}=25$ its value is around 35%). From the CASCADITA simulation we also note that the detection efficiency of the PPLF evolves with the value of its reconstructed charge: the better efficiency (90% of the charge) is obtained for charges $Z_{\mathrm{PPLF}}=20-23$ and is of the order of 60–85% for the lower and higher charges. In the following, in order to study only events with a good detection efficiency and a low contamination, we will select events with a PPLF reconstituted charge satisfying the condition

$$17\leq Z_{\mathrm{PPLF}}\leq 20 . \quad (3)$$

With this additional condition, only 10% of the initial events are finally retained (the final sample consists of around 700 000 events). The PPLF mean velocity of the selected events is about 6.6 cm/ns (the beam velocity is 8.2 cm/ns). The accuracy of the reconstructed velocity determined from the simulation is around 10%.

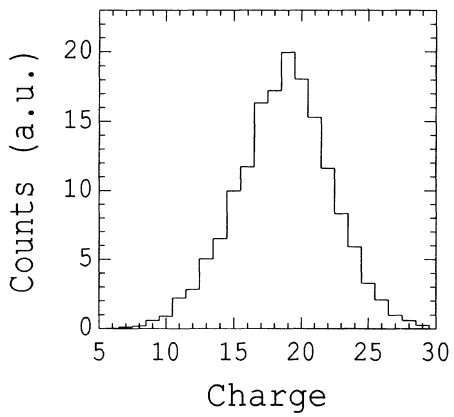

FIG. 3. Charge distribution of the PPLF reconstituted from the experimental data.

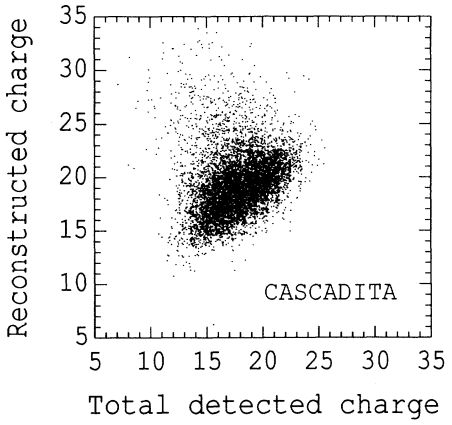

FIG. 4. Reconstructed PPLF charge versus the total detected charge of the PPLF decay products, calculated within the CASCADITA simulation.

According to CASCADITA, the selected quasicomplete PPLF events correspond on the average to impact parameters of 5.6 fm, the FWHM of the distribution being 2 fm. Experimentally the impact parameter can roughly be estimated from a measured global variable such as the total multiplicity of detected particles. The method we used for determining impact parameter [30] is based on the assumptions that the total cross section is purely geometrical ($\sigma_T=\pi b^2$) and that there is a (strong) monotonic correlation between multiplicity and impact parameter. This method was first proposed for relativistic nucleus-nucleus collisions and then applied to intermediate energy heavy ion reactions [31]. For the reaction under study, the maximum impact parameter deduced from the total reaction cross section given by the semiempirical parametrization of Kox *et al.* [32] is 9.3 fm. For our sample of events, we estimated an impact parameter mean value of 5.4 fm, which is in good agreement with the simulation prediction (the FWHM of the experimental distribution is around 3.5 fm).

IV. PPLF CHARACTERISTICS

A. Excitation energy

From the knowledge (charge, mass, kinetic energy, and direction of emission) of all charged particles attributed to the PPLF, we can estimate event by event its excitation energy. The excitation energy in any given event was estimated as

$$E^*=\sum_k E_k-Q+E_n , \quad (4)$$

where the E_k are the measured kinetic energies of the particles in the PPLF reference frame. The evaluation of the Q value was made using the most stable isotope for the nonidentified masses ($Z\geq 3$). A small correction for unobserved neutrons (E_n) was made using an average

multiplicity of neutrons calculated in order to reconstitute the most stable isotope associated with the PPLF charge and an average kinetic energy per neutron equal to $2T$. The temperature T was estimated by the relation $E_1^* = A/8T^2$, where E_1^* is the excitation energy calculated in a first step from the energies E_k and the Q value. The multiplicity of neutrons represents on the average about 75% of the proton multiplicity. The mean excitation energy is around 120 MeV and energies up to 300–350 MeV are obtained (Fig. 5). The excitation energy distribution exhibits some peaks in the low-energy domain, which correspond to the various charge partitions involving one heavy fragment and a few protons and/or α particles [33]. The method for calculating the excitation energy was again verified by the CASCADITA simulation. The simulation shows that there is a strong correlation between the reconstructed PPLF excitation energy (or velocity) and the impact parameter. The calculated excitation energies seem to be on the whole underestimated. At 100 MeV, the accuracy on the extracted value is around 30% but becomes better than 10% above 200 MeV. At low excitation energy (below 50 MeV), the estimated excitation energy is, on the average, strongly underestimated, and the accuracy is of the order of 50%. In the following, on account of this inaccuracy of the method at low excitation energy, we will discard events with excitation energy lower than 50 MeV.

For each excitation energy bin of 50 MeV between 50 and 250 MeV, the characteristics of the PPLF were calculated, namely, its mean excitation energy, mean velocity, and mean deflection angle (Table I). We did not analyze events of excitation energy greater than 250 MeV on account of their poor statistics. Averaged impact parameters estimated for each excitation energy bin from the multiplicities are also displayed in Table I. We can see that the PPLF velocity decreases as the excitation energy increases, whereas the deflection angle increases, as expected for more and more dissipative collisions. The corresponding impact parameter value varies from 6.5 to 3.6 fm. The low-excitation-energy events are associated with peripheral collisions, while the higher-energy events correspond rather to intermediate impact parameter (mid-peripheral) collisions.

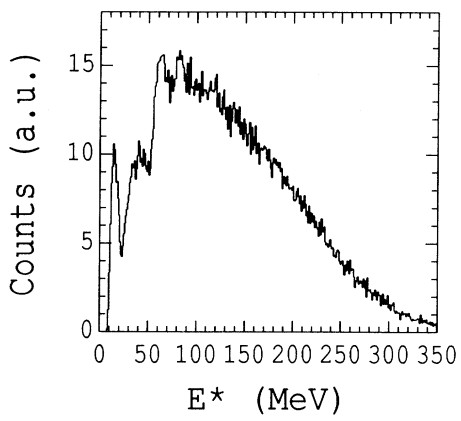

FIG. 5. Excitation energy distribution determined from the experimental data for PPLF of charge between 17 and 20.

TABLE I. Averaged PPLF excitation energy, velocity, deflection angle, angular momentum, and associated impact parameter as a function of the excitation-energy bin.

Energy bin (MeV)	$\langle E^* \rangle$ (MeV)	$\langle v \rangle$ (cm/ns)	$\langle \theta \rangle$ (deg)	$\langle L \rangle$ ($\hbar$)	$\langle b \rangle$ (fm)
50–100	76	7.0	6.7	12±0.5	6.5
100–150	124	6.6	7.6	18±1.0	5.7
150–200	173	6.3	8.7	23±1.5	4.6
200–250	222	6.0	9.5	30±2.0	3.6

B. Angular momentum

The extraction of the PPLF angular momentum involves the determination of the reaction plane. The reaction plane is defined, event by event, by the directions of the PPLF velocity and of the beam. Once again the accuracy of the procedure was verified using simulated (CASCADITA) data, which showed that the reaction plane is correctly determined on the average. The maximum error is ±30°. This value is smaller than that found by Wilson *et al.* from azimuthal correlations [34]. We suppose that the angular momentum of the PPLF is directed perpendicularly to the reaction plane. If this is the case, the tendency for light-emitted particles to remove angular momentum produces some focusing in the reaction plane.

To estimate angular momentum, we have compared the experimental angular distributions of the particles emitted by the PPLF (with respect to its reconstituted center-of-mass reference frame) to the predictions of a multistep Hauser-Feshbach Monte Carlo simulation code (LANCELOT) of the evaporation process [13]. In this code the angular distributions of the emitted particles are calculated in the framework of the Ericson and Strutinski [35] semiclassical method. The evaporation calculations were performed for excited ^{40}Ca nuclei having the different experimental kinematical configurations ($\langle E^* \rangle, \langle v \rangle, \langle \theta \rangle$) given in Table I and for different angular-momentum values ranging from 0 to 35$\hbar$. The LANCELOT events were filtered by the AMPHORA response, and the angular distributions were determined for events where the total detected charge is between 17 and 20 and for particles satisfying the conditions of adherence to the PPLF's described in the preceding section. We have verified that such a selection does not affect, on the average, the excitation energy, the velocity, and the deflection angle of the reconstructed initial excited nucleus.

The experimental α-particle angular distributions obtained for the different excitation energy bins are plotted in Fig. 6. The spectra represent the distribution of the particles with respect to the normal to the reaction plane. We observe that the particles are preferentially emitted in the vicinity of the reaction plane and that the angular anisotropy increases with the excitation energy. In fact, for the four energy bins, the ratios of the maximum value of

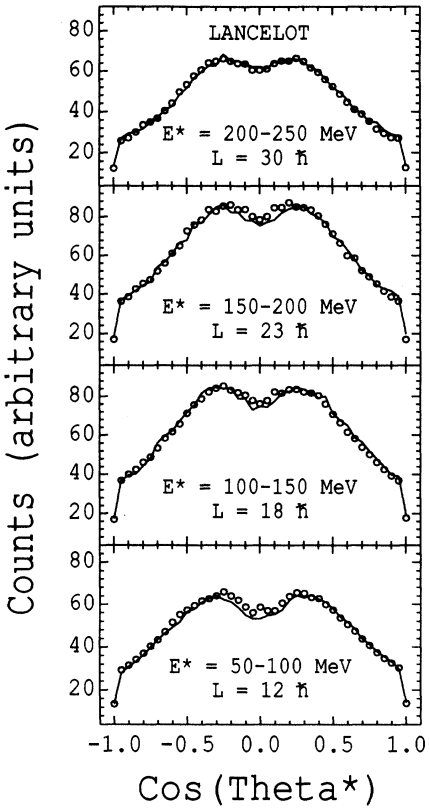

FIG. 6. Experimental alpha particle angular distributions obtained for the different excitation-energy bins (circles) and corresponding distributions calculated with the LANCELOT code (lines). They represent the distribution of the cosine of the relative angle (labeled Theta*) between the direction of emission and the normal to the reaction plane.

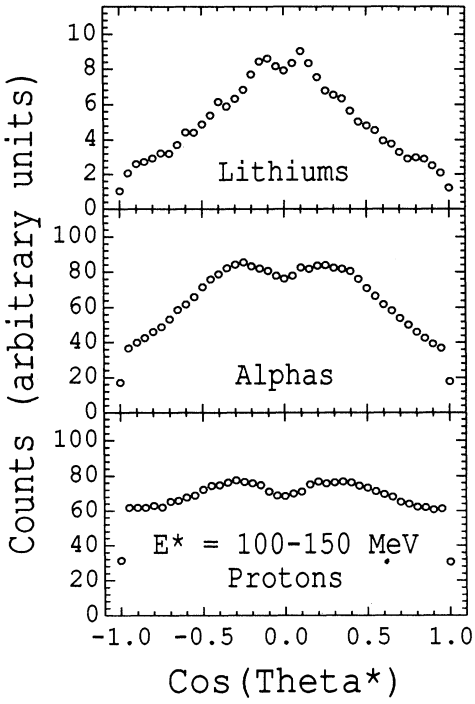

FIG. 7. Experimental angular distributions of protons, alphas and lithiums for the (100–150) MeV excitation energy bin.

the angular distribution with respect to its minimum value are 4.9 (50–100 MeV), 5.0 (100–150 MeV), 5.1 (150–200 MeV), and 5.3 (200–250 MeV). One can think that this effect reflects increasing PPLF angular momentum. The counting reduction observed around $\cos\theta^*=0$ (reaction plane) corresponds to the very forward angular domain in the laboratory (0°–4°), which is not covered by the AMPHORA array (beam passage). Figure 7 shows angular distributions for protons, alphas, and lithiums for the intermediate excitation energy bin. We can see that the in-plane focusing strongly increases with the charge of the emitted particle.

For each excitation energy bin, we have compared the experimental α-particle angular spectrum to the distributions given by the code LANCELOT. The angular anisotropy of α particles being more pronounced than for protons, this makes the comparison with theory easier (lithium particles and heavier particles are not included in the code). The angular momentum values obtained for each excitation energy bin are given in Table I. The uncertainties come from the fit of the experimental angular distributions by LANCELOT. The corresponding LANCELOT α-particle angular distributions are plotted in Fig. 6. The effect of the detection filter and selection method on the (LANCELOT) angular distribution of α particles evaporated from a PPLF having an excitation energy of 124 MeV, an angular momentum of $18\hbar$, a velocity of 6.6 cm/ns, and an emission angle of 7.6° is presented in Fig. 8. The main effect is a drastic diminution of the counting (by a factor of 5). We observe also a slight broadening of the distribution as well as the reduction around the reaction plane already mentioned.

As far as we know, this work on evaporated light-particle angular distributions constitutes the first attempt of determining angular momentum from reconstituted

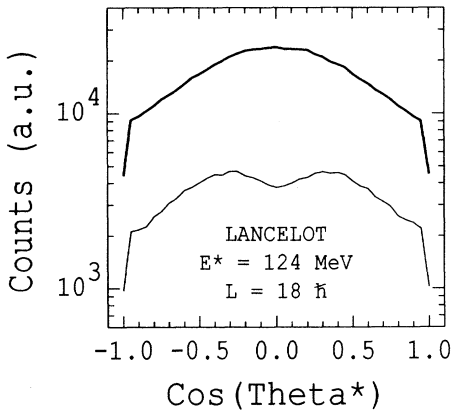

FIG. 8. Alpha angular distributions from LANCELOT calculations before (thick line) and after (thin line) filtering and selection (see text).

emitting nuclei. A somewhat similar analysis of particle angular distributions was recently done at GANIL energies in order to extract the angular momentum of fissile quasitargets, which were characterized by detection of the two PTLF fission products [36].

V. COMPARISON WITH MODELS

A. Excitation energy and angular momentum

The PPLF excitation energy and angular-momentum extracted values are compared with the predictions of two simple nucleus-nucleus collision models. The first one is a classical trajectory model (code MTC) [37], which contains conservative and dissipative forces (phenomenological Coulomb potential [7], proximity nuclear potential [38], and proximity one-body nuclear friction [39]). The friction force allows energy and angular-momentum transfer between the two colliding nuclei. Mass transfer is not considered. For a given value of impact parameter, the trajectory of the system is followed as a function of time. The system can fuse if the ions are trapped behind a potential barrier or scatter if they escape over the barrier. For the reaction under study, the MTC calculations lead to fusion for impact parameters lower than 1.7 fm. Within the assumption of a purely geometrical cross section, fusion represents about 3% of the total cross section. The second model is the nuclear random walk model (code PERCUTE) [9]. In this model, the ion-ion interaction is assumed to be governed by the number of nucleon-nucleon collisions taking place along the trajectory of the system. Nucleon-nucleon collisions generate some variation in the masses of the projectile and targetlike fragments as well as emission of nucleons to the continuum. The kinetic energy loss from the projectile is given by the number of nucleon-nucleon collisions. This energy dissipation appears partly as excitation energy of the two fragments and partly as recoil kinetic energy of the targetlike fragment and of the emitted nucleons. Angular momentum is imparted to the fragments by the absorbed nucleons. The mass changes are generated using a matrix of probabilities, which are free parameters of the model. The numerical values of these parameters we have used were taken from a study of the $^{20}Ne+^{165}Ho$ reaction at 30 MeV/nucleon [40].

In both models, we have considered two extreme cases for the excitation energy sharing between the primary projectile and targetlike fragments: equal partition of excitation energy and equal temperature (the total energy is shared in proportion to the mass). Since a large range of excitation energies are involved in our study, it is interesting to investigate the evolution of the excitation energy partition as a function of the degree of heating of the system, by comparing the data to the predictions given within these two assumptions. Recent results [41–43] have shown that the excitation energy partition between PPLF and PTLF evolves from energy equipartition for small dampings to a sharing close to thermal equilibrium for highly damped collisions. Such a behavior reflects an increasing interaction time that allows thermal equilibrium to be reached.

The PPLF angular momenta calculated in the framework of the MTC and PERCUTE codes are plotted in Fig. 9 vs the PPLF excitation energy, and are compared to the experimental values. The two models lead to neighboring curves up to 150–200 MeV. Above, the results are quite different: the one-body friction model gives lower angular momenta than the nucleon-nucleon collision model and the deviation between the two models increases with excitation energy. Such a discrepancy could be partially due to the absence of mass transfer in the MTC code. For both models, for a given PPLF excitation energy, the equipartition calculations lead to lower angular momenta than the equilibrium results, since the projectile nucleus is lighter than the target one. The experimental values are in good agreement with both models up to the 173 MeV point while the last point (222 MeV) is rather close to the PERCUTE predictions. Furthermore, the measurements seem to be in better agreement with the MTC curves calculated within the equipartition assumption for the 76 MeV point and within the equal temperature hypothesis for the 173 MeV point, the 124 MeV point being between the two curves. The 222 MeV point is close to the PERCUTE calculation performed in the thermal equilibrium case. Our results are therefore in agreement with the excitation energy partition evolution (from equipartition to thermal equilibrium) which was observed in earlier works [41–43].

B. Multiplicity and charge distributions

We have compared the multiplicity and charge distributions of the PPLF deexcitation products to the statistical Monte Carlo code GEMINI [15], which treats the deexcitation process of excited nuclei via a sequence of binary decays. All possible binary channels from light-particle emission to symmetrical division are considered. For the evaporation of light particles ($Z \leq 2$), the decay width is

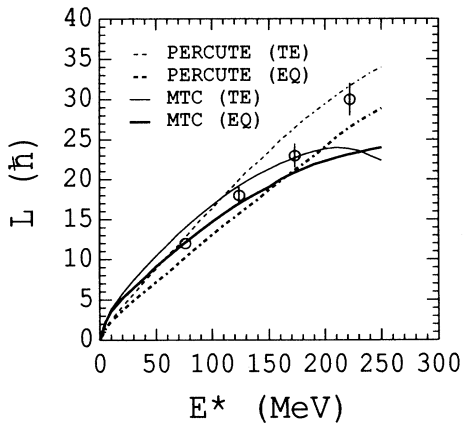

FIG. 9. PPLF angular momentum as a function of its excitation energy extracted from experiment (points) and calculated with the MTC (solid lines) and PERCUTE (dashed lines) codes. The thick lines represent the equipartition calculations (EQ) of the excitation energy sharing between PPLF and PTLF and the thin lines correspond to the thermal equilibrium predictions (TE).

calculated using the Hauser-Feshbach formalism [14]. For emission of heavier fragments, the decay width is determined using the transition state formalism of Moretto [16].

The experimental multiplicity and charge distributions obtained for each excitation energy bin are presented in Figs. 10 and 11, respectively. Between the two extreme energy bins, the mean multiplicity evolves from 3.8 to 7.4 (Fig. 10). In Fig. 11, we can see that the heavier charges progressively vanish with increasing excitation energy, whereas the production of intermediate charges increases strongly. Between the 50–100 MeV and 200–250 MeV bins, the production rate of intermediate mass fragments increases by a factor of 4 with respect to the light-particle production.

The GEMINI calculations were performed for excited ^{40}Ca nuclei having the different experimental averaged characteristics ($\langle E^* \rangle$, $\langle v \rangle$, $\langle \theta \rangle$, and $\langle L \rangle$) given in Table I. The calculated samples were, as for the LANCELOT event analysis, filtered by the detection apparatus response. The multiplicity and charge distributions of the decay products were determined for events having a total detected charge included between 17 and 20 and for particles fulfilling the conditions of adherence to the PPLF. The obtained theoretical distributions are plotted in Figs. 10 and 11 to be compared to the experimental data. We note that the multiplicity spectra are very well reproduced by the GEMINI code, whatever the excitation-energy bin. For the charge distributions, the code underestimates the production of intermediate mass fragments at low excitation energy (50–100-MeV bin) and moves to better agreement at higher energies. For the higher-excitation-energy bin (200–250 MeV), the experimental data are remarkably well reproduced by the simulation. The discrepancy observed for the lower-energy bin (50–100 MeV) between the experimental and GEMINI charge distributions could arise from the inaccuracy at low energy of the excitation-energy calculating method, which was mentioned above.

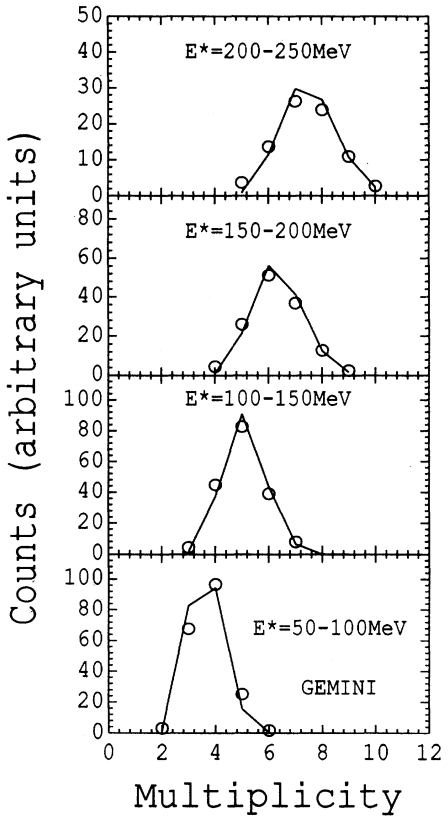

FIG. 10. Experimental multiplicity distributions of the particles and fragments assigned to the PPLF for the different excitation-energy bins (circles) and corresponding GEMINI distributions (lines). For each bin, the experimental and simulated curves correspond to the same number of events.

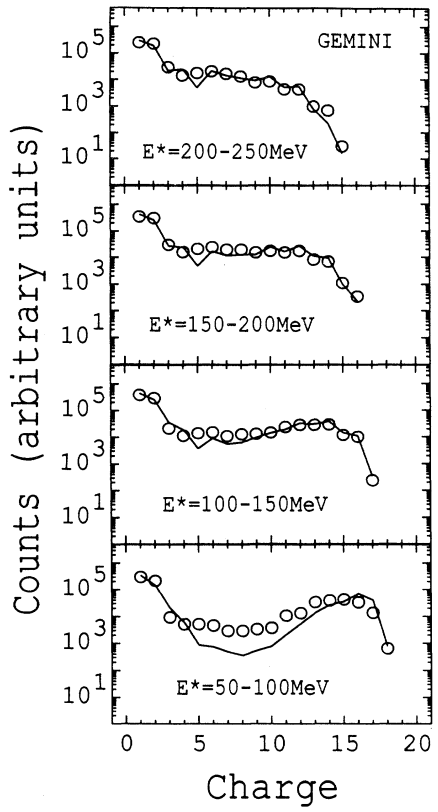

FIG. 11. Experimental charge distributions of the PPLF decay products for the different excitation energy bins (circles) and corresponding GEMINI distributions (lines). For each bin, the experimental and simulated curves correspond to the same number of events.

VI. SUMMARY AND CONCLUSIONS

In this work, we have studied, with the AMPHORA array, primary projectilelike fragments produced in the reaction ^{40}Ca+^{nat}Cu at 35 MeV/nucleon. Such measurements have enabled the selection of binary events with quasicomplete detection of the PPLF decay products, and reconstruction of its center-of-mass velocity, its total charge, its excitation energy and the reaction plane.

Simulations based on simple nucleus-nucleus collision and statistical decay models associated with event filtering by the detection constraints have shown the validity of the selection-reconstruction proposed method. From the analysis of the total multiplicities, the selected events have been associated with semiperipheral and peripheral collisions (impact parameters in the range 3–7 fm).

The PPLF excitation-energy spectrum extends to very high energies (up to 8 MeV/nucleon). The PPLF angular momentum has been estimated by comparing the α-particle center-of-mass angular distributions with respect to the reaction plane with a Monte Carlo evaporation code. Angular-momentum values up to $30\hbar$ have been extracted. They are in rather good agreement with both one-body friction and nucleon-nucleon collision model calculations, and the sharing of the excitation energy between the primary projectile and targetlike fragments is found to be consistent with an evolution with excitation energy from energy equipartition towards a repartition close to thermal equilibrium.

The multiplicity and charge distributions of the PPLF decay products are in good agreement with the predictions of a sequential binary decay model whatever the excitation energy. We do not observe a change of the deexcitation mechanism as the excitation energy increases. Our results suggest, in agreement with our previous analysis of momentum ellipsoids [11], that the critical region (in the percolation sense), which was found close to 5 MeV/nucleon from the analysis of charge partitions, is not associated with a transition towards a prompt multifragmentation process. The observed increasing production of intermediate mass fragments with excitation energy is, according to the present analysis, driven by centrifugal forces.

[1] Ch. Egelhaaf, M. Bürgel, H. Fuchs, A. Gamp, H. Homeyer, D. Kovar, and W. Rauch, Nucl. Phys. **A405**, 397 (1983).

[2] D. Guerreau, V. Borrel, D. Jacquet, J. Galin, B. Gatty, and X. Tarrago, Phys. Lett. **131B**, 293 (1983).

[3] F. Rami, J. P. Coffin, G. Guillaume, B. Heusch, P. Wagner, A. Fahli, and P. Fintz, Nucl. Phys. **A444**, 325 (1985).

[4] R. Dayras, A. Pagano, J. Barrette, R. Berthier, D. M. De Castro Rizzo, E. Chavez, O. Cisse, R. Legrain, M. C. Mermaz, E. C. Pollacco, H. Delagrange, W. Mittig, B. Heusch, R. Coniglione, G. Lanzano, and A. Palmeri, Nucl. Phys. **A460**, 299 (1986).

[5] M. Stern, R. Billerey, B. Chambon, A. Chbihi, A. Chevarier, N. Chevarier, B. Cheynis, D. Drain, C. Pastor, J. Alarja, A. Dauchy, A. Giorni, D. Heuer, C. Morand, and J. B. Viano, Z. Phys. A **331**, 323 (1988).

[6] J. Pouliot, Y. Chan, D. E. DiGregorio, B. A. Harmon, R. Knop, C. Moisan, R. Roy, and R. G. Stokstad, Phys. Rev. C **43**, 735 (1991).

[7] J. P. Bondorf, M. I. Sobel, and D. Sperber, Phys. Rev. C **15**, 83 (1974).

[8] J. N. De, D. H. E. Gross, and H. Kalinowski, Z. Phys. A **277**, 385 (1976).

[9] A. J. Cole, Phys. Rev. C **35**, 117 (1987); A. J. Cole, R. Cherkaoui-Tadili, and J. Alarja, *ibid.* **40**, 1265 (1989).

[10] Y. Yariv and Z. Fraenkel, Phys. Rev. C **20**, 2227 (1979).

[11] P. Désesquelles, A. J. Cole, A. Giorni, D. Heuer, A. Lleres, J. B. Viano, B. Chambon, B. Cheynis, D. Drain, and C. Pastor, Phys. Rev. C **48**, 1828 (1993).

[12] F. Puhlhofer, Nucl. Phys. **A280**, 267 (1977).

[13] A. J. Cole, N. Longequeue, J. Menet, J. J. Lucas, R. Ost, and J. B. Viano, Nucl. Phys. **A341**, 284 (1980).

[14] T. D. Thomas, Annu. Rev. Nucl. Sci. **18**, 343 (1968).

[15] R. J. Charity, M. A. McMahan, G. J. Wozniak, R. J. McDonald, and L. G. Moretto, Nucl. Phys. **A483**, 371 (1988).

[16] L. G. Moretto, Nucl. Phys. **A247**, 211 (1975).

[17] B. Borderie, Ann. Phys. (Paris) **17**, 349 (1992).

[18] Zhang Xiao-Ze, D. H. E. Gross, Xu Shu-Yan, and Zheng Yu-Ming, Nucl. Phys. **A461**, 641 (1987); **A461**, 668 (1987).

[19] W. A. Friedman, Phys. Rev. C **42**, 667 (1990).

[20] D. Drain *et al.*, Nucl. Instrum. Methods Phys. Res. A **281**, 528 (1989).

[21] D. W. Stracener, D. G. Sarantites, L. G. Sobotka, J. Elson, J. T. Hood, Z. Majka, V. Abenante, A. Chbihi, and D. C. Hensley, Nucl. Instrum. Methods Phys. Res. A **294**, 485 (1990).

[22] M. E. Brandan, A. J. Cole, P. Désesquelles, A. Giorni, D. Heuer, A. Lleres, A. Menchaca-Rocha, and K. Michaelian, Nucl. Instrum. Methods Phys. Res. A **334**, 461 (1993).

[23] A. Menchaca-Rocha, E. Garcia-Solis, E. Belmont-Moreno, M. E. Brandan, M. Buenerd, J. Chauvin, P. DeSaintignon, G. Duhamel, D. Lebrun, P. Martin, G. Perrin, and J. Y. Hostachy, Phys. Rev. C **45**, 1189 (1992); A. Menchaca-Rocha, E. Garcia-Solis, and K. Michaelian, Rev. Mexicana Fis. **38**, Supl. **2**, 114 (1992).

[24] A. Fahli, J. P. Coffin, G. Guillaume, B. Heusch, F. Jundt, F. Rami, P. Wagner, P. Fintz, A. J. Cole, S. Kox, and Y. Schutz, Phys. Rev. C **34**, 161 (1986).

[25] Code BINFRAG, A. J. Cole, R. Cherkaoui-Tadili, and J. Alarja, Phys. Rev. C **40**, 1265 (1989). See also K. Grotowski, J. Ilnicki, T. Kozik, J. Lukasik, S. Micek, Z. Sosin, A. Wieloch, N. Heide, H. Jelitto, I. Kiener, H. Rebel, S. Zagromski, and A. J. Cole, Phys. Lett. B **223**, 287 (1989).

[26] M. Blann, Phys. Rev. C **31**, 1245 (1985).

[27] B. Cheynis, B. Chambon, D. Drain, C. Pastor, D. Heuer, A. Dauchy, A. Giorni, C. Morand, and P. Stassi, Z. Phys. A **335**, 77 (1990).

[28] A. Giorni, A. J. Cole, P. Désesquelles, H. Elhage, D. Heuer, A. Lleres, P. Stassi, J. B. Viano, F. Benrachi, B. Chambon, B. Cheynis, D. Drain, and C. Pastor, in *Proceedings of the International Conference on New Nuclear Physics with Advanced Techniques, Ierapetra, 1991,* edited by F. Beck, S. Kossionides, and C. Kalfas (World Scientific, Singapore, 1992), p. 312; *Proceedings of the Tours Symposium on Nuclear Physics, Tours, 1991,* edited by M. Ohta and B Rémaud (World Scientific, Singapore, 1992), p. 87.

[29] H. Elhage, Doctoral thesis, Université Joseph Fourier Grenoble-1 France, 1992.

[30] C. Cavata, M. Demoulins, J. Gosset, M. C. Lemaire, D. Lhôte, J. Poitou, and O. Valette, Phys. Rev. C **42**, 1760 (1990).

[31] L. Phair, W. Bauer, D. R. Bowman, N. Carlin, R. T. DeSouza, C. K. Gelbke, W. G. Gong, Y. D. Kim, M. A.

Lisa, W. G. Lynch, G. F. Peaslee, M. B. Tsang, C. Williams, F. Zhu, N. Colonna, K. Hanold, M. A. McMahan, G. J. Wozniak, and L. G. Moretto, Phys. Lett. B **285**, 10 (1992).

[32] S. Kox, A. Gamp, C. Perrin, J. Arvieux, R. Bertholet, J. F. Bruandet, M. Buenerd, R. Cherkaoui, A. J. Cole, Y. El-Masri, N. Longequeue, J. Menet, F. Merchez, and J. B. Viano, Phys. Rev. C **35**, 1678 (1987).

[33] P. Désesquelles, Doctoral thesis, Université Joseph Fourier Grenoble-1 France, 1991.

[34] W. K. Wilson, R. Lacey, C. A. Ogilvie, and G. D. Westfall, Phys. Rev. C **45**, 738 (1992).

[35] T. Ericson and V. Strutinski, Nucl. Phys. **8**, 284 (1958).

[36] G. Bizard, J. Colin, and Ch. Meslin, Report No. LPCC 93-04, Laboratoire de Physique Corpusculaire, Caen France, 1993.

[37] J. R. Birkelund, L. E. Tubbs, J. R. Huizenga, J. N. De, and D. Sperber, Phys. Rep. **56**, 107 (1979).

[38] J. Blocki, J. Randrup, W. J. Swiatecki, and C. F. Tsang, Ann. Phys. **105**, 427 (1977).

[39] J. Randrup, Ann. Phys. **112**, 356 (1978).

[40] J. Alarja, Doctoral thesis, Université Joseph Fourier Grenoble-1 France, 1988.

[41] J. L. Wile, S. S. Datta, W. U. Schröder, J. R. Huizenga, J. Tôke, and R. T. DeSouza, Phys. Rev. C **39**, 1845 (1989).

[42] K. Kwiatkowski, R. Planeta, S. H. Zhou, V. E. Viola, H. Breuer, M. A. McMahan, and A. C. Mignerey, Phys. Rev. C **41**, 958 (1990).

[43] D. Jouan, B. Borderie, M. F. Rivet, C. Cabot, H. Fuchs, H. Gauvin, C. Gregoire, F. Hanappe, D. Gardes, M. Montoya, B. Remaud, and F. Sebille, Z. Phys. A **340**, 63 (1991).